

Open-Structured Nanotubes with Three-Dimensional Ion-Accessible Pathways for Enhanced Li⁺ Conductivity in Composite Solid Electrolytes

Song Hu, Lulu Du, Gang Zhang, Wenyuan Zou, Zhe Zhu, Lin Xu,* and Liqiang Mai

Cite This: <https://dx.doi.org/10.1021/acsami.0c22635>

Read Online

ACCESS |

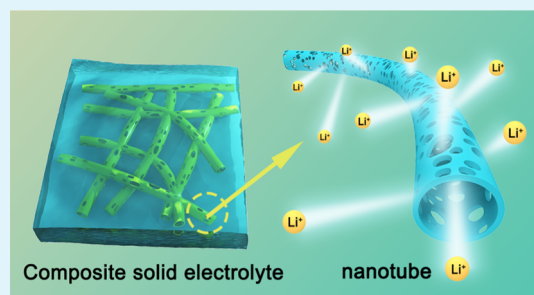
Metrics & More

Article Recommendations

Supporting Information

ABSTRACT: Composite solid electrolytes (CSEs) hold great promise toward safe lithium metal batteries with high energy density, due to integration of the merits of polymer matrixes and fillers. Rational design of filler nanostructures has attracted increasing attention for improving the ionic transport of CSEs in solid batteries. In this work, we fabricated open-structured Li_{0.33}La_{0.557}TiO₃ (LLTO) nanotubes (NTs) as ion-conductive fillers in CSEs by a gradient electrospinning method for the first time. Different from nanoparticles (NPs) and nanowires (NWs), our nanotubes are composed of connected small NPs, which offer three-dimensional (3D) Li⁺-accessible pathways, large polymer/filler interfacial ionic conduction regions, and enhanced wettability against the polymer matrix. As a result, the solid electrolytes based on LLTO NTs and polyacrylonitrile (PAN) can display a high ionic conductivity of up to $3.6 \times 10^{-4} \text{ S cm}^{-1}$ and a wide electrochemical window of 5 V at room temperature (RT). Furthermore, Li–Li symmetric cells using the LLTO NTs/PAN CSE can work stably over 1000 h with a polarization of 20 mV. LiFePO₄–Li full cells exhibit a high capacity of 142.5 mAh g⁻¹ with a capacity retention of 90% at 0.5 C after 100 cycles. All of these results demonstrate that the design of open-structured nanotubes as fillers is a promising strategy for high-performance solid electrolytes.

KEYWORDS: composite solid electrolytes, nanoparticles, room temperature, nanotubes, polyacrylonitrile



1. INTRODUCTION

To meet the increasing demand of the consumer electronics market, the development of efficient and safe energy storage equipment has been paid more and more attention.^{1,2} As the most common energy storage device, lithium-ion batteries have been widely studied and used in daily life.^{3,4} However, commercial liquid electrolytes have risks of leakage and fire hazard because of their intrinsic flammability as well as safety problems caused by lithium dendrite penetration.⁵ To solve these problems with liquid electrolytes, it is a promising strategy to develop novel solid-state batteries with solid electrolytes.⁶ Compared with conventional liquid electrolytes, solid electrolytes can not only realize high-safety batteries owing to their nonflammability and higher mechanical strength but also improve the energy density of lithium-ion batteries by matching lithium metal anodes.^{7,8} As one of the most common solid electrolytes, polymer-based solid electrolytes have drawn increasing attention because of their facile manufacture and benign contact with electrodes.^{9,10} Unfortunately, their low ionic conductivity and poor mechanical properties inhibit their further application.¹¹ Inorganic electrolytes are another important class of solid electrolytes is, which usually show high ionic conductivity and a wide electrochemical stability window. They have the potential to couple with Li metal and high-voltage cathodes to improve the energy density of solid

batteries.^{12,13} However, they are fragile and suffer from poor interface contact with the electrodes, which needs further improvement.^{14–16} To fabricate high-performance solid electrolytes in terms of high ionic conductivity and benign contact with electrodes, an effective approach is to prepare composite solid electrolytes (CSEs), which can integrate the advantages of polymers and inorganic solid electrolytes.^{17–19}

In comparison with polymer-based solid electrolytes, the introduction of fillers can generate good interaction with the polymer matrix, which facilitates the migration of lithium ions and thus enhances the ionic conductivity in composite solid electrolytes.^{20,21} Besides, the addition of fillers can also effectively improve the thermal performance and mechanical strength of the CSEs.²² In most reported works, fillers can be divided into non-Li⁺-conductive nanoparticles, such as Al₂O₃,²³ TiO₂,²⁴ and SiO₂,²⁵ and Li⁺-conductive nanoparticles, including LLTO,¹⁸ Li₇La₃Zr₂O₁₂,²⁰ and Li_{1.3}Al_{0.3}Ti_{1.7}(PO₄)₃.²⁶

Received: December 22, 2020

Accepted: February 26, 2021

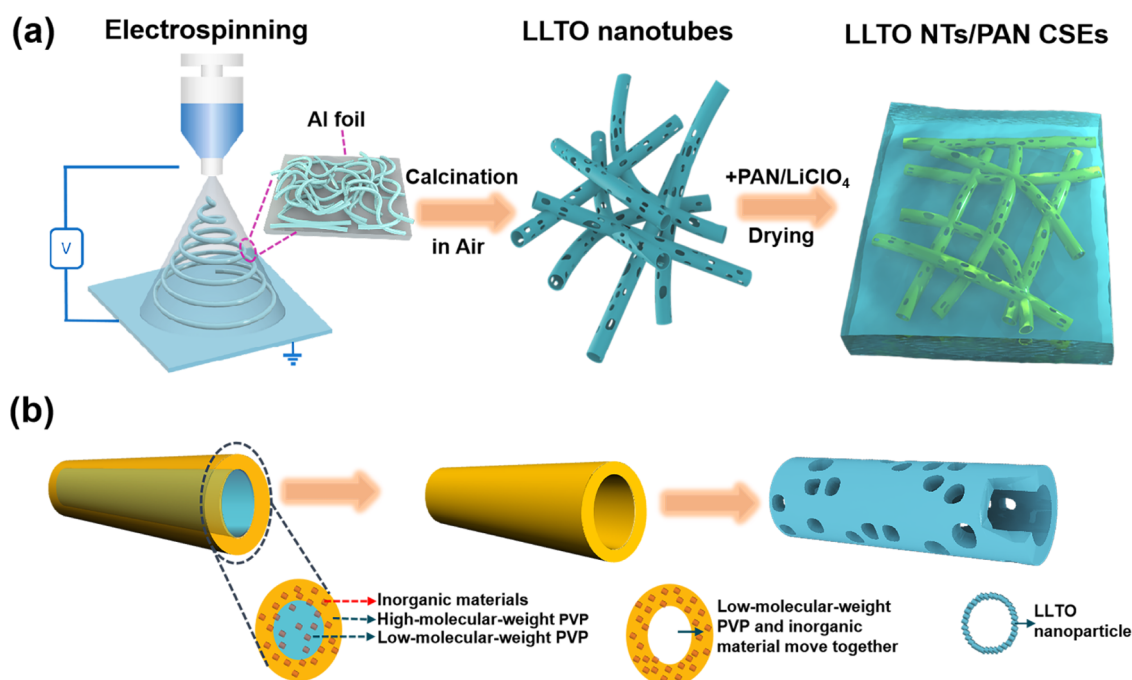


Figure 1. Material synthesis. (a) Schematic of fabrication procedures of LLTO NTs/PAN CSEs. (b) Schematic of the LLTO NT formation process.

However, nanoparticles are usually dispersed randomly in solid electrolytes, making it difficult to form continuous ionic transport pathways.

Developing rational nanostructured fillers is a brilliant approach to take full use of their advantages, because it extends ion transport pathways and improves the interaction between fillers and the polymer matrix.^{27,28} A typical one is a nanowire. Cui groups rationally constructed LLTO nanowires incorporated in solid electrolytes, which showed enhanced ionic conductivity.²⁹ This result indicates that fillers with a one-dimensional structure and a high aspect ratio can provide long-term and continuous lithium ion transport, forming fast conductive networks in contrast to randomly dispersed nanoparticles. Another approach is to introduce pores on the surface of fillers to improve the wettability against the polymer matrix.³⁰ The improvement of wettability helps infiltration of polymer-based electrolytes into the pores to form more effective interface contact areas with fillers.³¹ This promotes the Lewis acid-based interaction between the fillers and polymer electrolytes, resulting in the adsorption of anions of Li salts and release of more free Li⁺, thus remarkably boosting the ionic conductivity of the CSEs.³² A third approach is to increase the specific surface area of the fillers to enlarge the interfacial interaction regions with the polymer matrix, which plays an important role in the enhancement of the ionic conductivity.^{33–35} For instance, a porous SiO₂ aerogel was developed as the filler in a PEO-based electrolyte, and the SiO₂ aerogel could provide a large and continuous surface to form more interfacial regions, thereby facilitating fast Li⁺ conduction through the filler/polymer interface.²⁵ Therefore, exploring a well-designed nanostructure for fillers is an essential direction to obtain high-ionic-conductivity composite solid electrolytes for solid-state lithium metal batteries.

In this work, we successfully fabricated open-structured LLTO nanotubes (NTs) as ion conductors in composite solid electrolytes by a gradient electrospinning method for the first

time. Compared with nanoparticles and nanowires, these open-structured nanotubes are composed of connected small nanoparticles, providing three dimensional (3D) accessible pathways for lithium-ion transport. Besides, the pores on the surface improve the interface wettability between LLTO NTs and the polymer matrix, thus promoting the adsorption of anions. Apart from this, their large specific surface area increases interfacial ionic conduction regions in the as-obtained LLTO NTs/polyacrylonitrile (PAN) PAN CSE. With the reasonable design of the filler structure, the solid electrolyte composed of LLTO NTs and PAN achieves an ionic conductivity of $3.6 \times 10^{-4} \text{ S cm}^{-1}$ at room temperature (RT) coupled with highly enhanced electrochemical windows and mechanical strength. This solid electrolyte endows the assembled lithium symmetric battery with small polarization and long cycle life over 1000 h at a current density of 0.05 mA cm⁻². Good cycling stability and high rate capacity were also obtained for full cells with the LLTO NTs/PAN CSE against a LiFePO₄ cathode.

2. EXPERIMENTAL SECTION

2.1. Synthesis of LLTO Nanotubes. Appropriate amounts of LiNO₃, La(NO₃)₃·6H₂O, and Ti(OC₄H₉)₄ were dissolved in dimethylformamide (DMF) and acetic acid, and then high- and low-molecular-weight polyvinylpyrrolidone (LPVP) were added. After rapid stirring for 24 h, a transparent uniform precursor solution was obtained. Then nanowires were prepared from the precursor solution by electrospinning and were collected on aluminum foil. Finally, the as-spun nanowires were heated at different temperatures (700–850 °C) for 2 h in air to fabricate LLTO nanotubes.

2.2. Fabrication of LLTO NTs/PAN CSEs. LiClO₄, PAN, and an appropriate amount of LLTO NTs were dissolved in DMF. After stirring at 60 °C for 12 h, the well-stirred solution was poured into a petri dish and dried at 80 °C under vacuum for 12 h to remove the excess solvent. Finally, the dried film was quickly transferred to a glovebox for preservation. The detailed experimental procedures, electrochemical measurements, and characterization are shown in the Supporting Information.

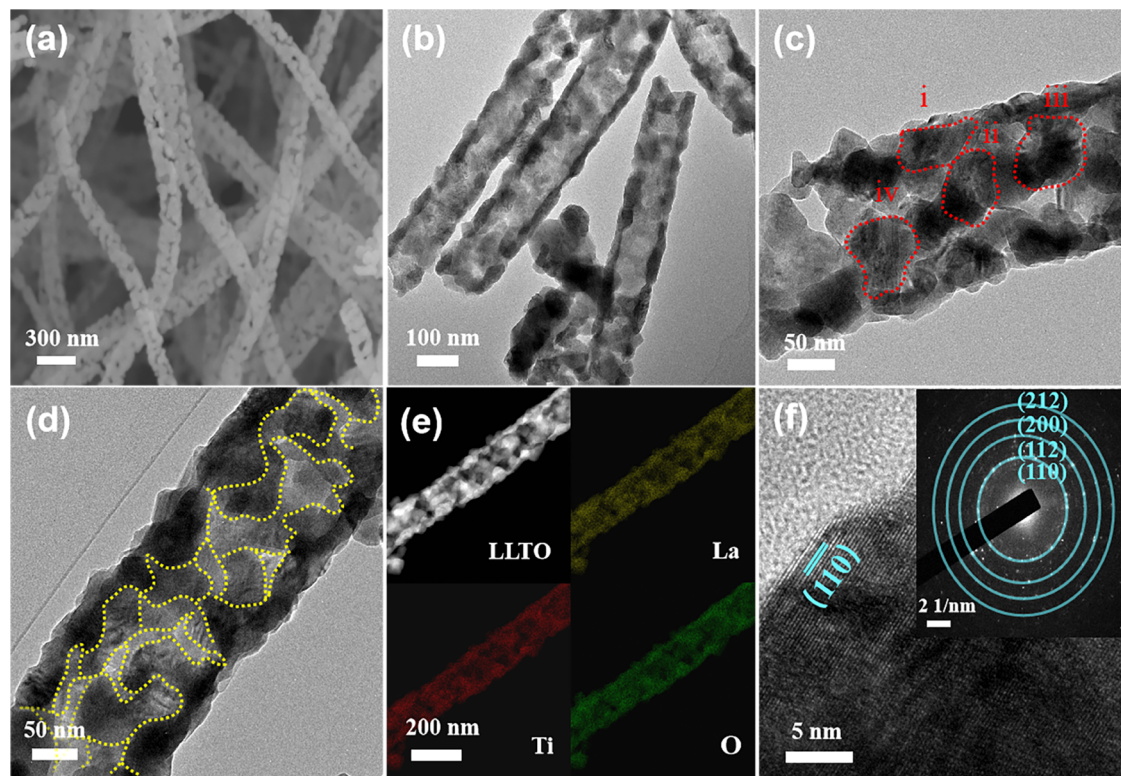


Figure 2. Structural characterization of LLTO NTs calcined at 800 °C. (a) SEM image. (b) TEM image. (c) TEM image of the head of a nanotube composed of NPs (i–iv). The yellow lines in (d) represent channels and voids formed among the NPs. (e) EDS elemental mappings of NTs. (f) HRTEM image and SAED pattern of NTs.

3. RESULTS AND DISCUSSION

As depicted in Figure 1a, LLTO NTs were prepared by a gradient electrospinning method, which is usually used to synthesize one-dimensional materials with a high aspect ratio.³⁶ The structure can be tailored by controlling the polymer composition in the precursor solution. To obtain LLTO with a nanotube structure, the optimal result was obtained using 1.5 g low-molecular-weight polyvinylpyrrolidone (LPVP) and 1.05 g high-molecular-weight polyvinylpyrrolidone (HPVP) as polymer carriers in the precursor solution. Theoretically, a polymer with a higher molecular weight has a greater viscosity compared with a low-weight polymer, which shows a wider terminal jet radius in the electrospinning process.^{36–38} Therefore, the HPVP was distributed in the outer layer of the as-spun nanowires and the LPVP mainly located in the center, thus forming a unique gradient structure. After electrospinning, the product collected on aluminum foil was calcined to obtain the final LLTO NTs. Rapid weight loss occurs over 400 °C in the pyrolysis process (Figure 1b). In this temperature range, the LPVP located in the center of the as-spun nanowires decomposed faster because of its higher decomposition rate than that of HPVP (Figure S1). Then, the inorganic ingredient of the precursor tended to move toward the external boundary with the contraction of LPVP, eventually forming a tubular structure. The pores on the surface were formed by the decomposition of the inorganic ingredient and the partial pyrolysis of HPVP. Finally, the obtained LLTO NTs were dispersed in PAN/LiClO₄ to fabricate composite solid electrolytes.

Figure S2a shows the X-ray diffraction (XRD) patterns of LLTO nanotubes calcined at different temperatures (700–850 °C). When the calcination temperature exceeds 800 °C, the

diffraction peaks of the as-obtained LLTO NTs are well indexed to the tetragonal-phase *P4/mmm* perovskite structure Li_{0.33}La_{0.557}TiO₃ (JCPDS: 01-87-0935).³⁹ Figure 2a shows the representative scanning electron microscopy (SEM) images of LLTO NTs, showing the porous one-dimensional structure with a high aspect ratio, which can provide continuous and long-term Li⁺ transport pathways in the prepared solid electrolytes. Apart from this, transmission electron microscopy (TEM) images depicted in Figure 2b indicate the internal conditions of LLTO NTs, confirming that the fillers with distinct tubular structure and uniform size were successfully synthesized. The wall of LLTO NTs was composed of many small NPs of 30–50 nm in diameter (Figure 2c); the grain boundaries and pores are marked by yellow lines (Figure 2d). These NPs connected with each other and formed many pores and channels among NTs, providing an open structure and more 3D pathways for lithium-ions to access the extended interface. These pathways come from interfacial regions in pores, channels, and both outer and inner sides of LLTO NTs, which helps to improve the ionic conductivity of the composite solid electrolytes. These findings can be further confirmed by specific area tests of the LLTO NTs. The Brunauer–Emmett–Teller (BET) specific area of LLTO NTs (Figure S3) reached 11.73 m² g⁻¹, much higher than those of nanoparticles (2.58 m² g⁻¹) and nanowires (5.30 m² g⁻¹). Figure 2f shows the high-resolution TEM (HRTEM) image and selected area electron diffraction (SAED) pattern of LLTO NTs, in which measured interplanar distances are 2.72, 2.23, 1.94, and 1.58 Å, corresponding to the planes of (110), (112), (200), and (212), respectively. In addition, the corresponding energy dispersive X-ray spectrometry (EDS) elemental mapping of a single LLTO nanotube is shown in Figure 2e, revealing that La, Ti,

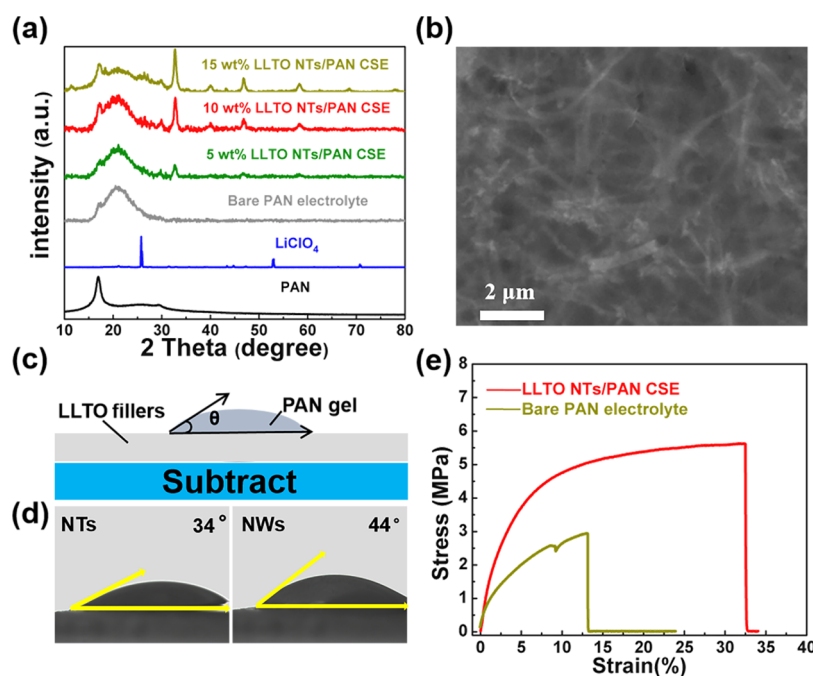


Figure 3. Characterization of LLTO NTs/PAN CSEs. (a) XRD patterns of PAN, LiClO_4 , and LLTO NTs/PAN CSEs with various concentrations of LLTO NTs. (b) SEM image of the LLTO NTs/PAN CSE. (c) Schematic of contact angle showing the wettability of reinforcements against the PAN-based polymer electrolyte and (d) the corresponding contact angle of NTs (left) and NWs (right). (e) Stress–strain curves of the LLTO NTs/PAN CSE and bare PAN solid electrolyte.

and O elements are uniformly distributed in this filler. Apart from this, the SEM images in Figure S4 show as-spun nanowires and LLTO NTs calcined at 700, 800, and 850 °C with corresponding average diameters of 242, 162, 140, and 130 nm. In the process of calcination, distinct nanotube structure is found to form at 700 °C and collapse at 850 °C, which may be caused by the overgrowth of LLTO grains. Therefore, with the open structure formed by exceptional connection of single NPs, the LLTO NT calcined at 800 °C was an optimal candidate because of its large specific surface area, high aspect ratio, and open structure, promising for use in the preparation of composite solid electrolytes and subsequent experiments.

Figure 3a shows the XRD patterns for PAN, LiClO_4 , and LLTO NTs/PAN CSEs containing different concentrations of LLTO NTs at RT. It is obvious that there is a characteristic diffraction peak of PAN around 17° and the diffraction peaks of LiClO_4 disappear in PAN-based electrolytes, which may be caused by its complete complexation with the PAN, indicating that there is no lithium salt particle remaining in the PAN-based electrolytes. The relative peak intensity of LLTO NTs/PAN CSEs shows no significant change with different amounts of LLTO NTs, suggesting that the addition of LLTO NTs has no obvious effect on the crystallinity of PAN. The SEM image of the solid electrolyte with 10 wt % LLTO NTs (10LLTO NTs/PAN CSE) shows LLTO NTs evenly distributed in the polymer-based electrolyte without agglomeration (Figure 3b), which contributes to fast lithium-ion transport. And the cross-sectional diagram of the 10LLTO NTs/PAN CSE in Figure S5 shows that the average film thickness is 220 μm . The surface structures and morphologies of the matrix can greatly affect the wettability of the liquid.⁴⁰ Based on this fact, the wettability of LLTO with different structures against polymer electrolytes was studied by measuring the contact angle (schematically shown in Figure 3c). As depicted in Figure 3d, the LLTO

nanotubes demonstrate a small contact angle of 33° against the PAN/ LiClO_4 electrolyte precursor solution, much smaller than that of LLTO nanowires (44°), which indicates the better wettability of LLTO nanotubes against the polymer matrix. The improvement of wettability is conducive to the penetration of PAN into the pores and surface of the LLTO nanotubes and thus to effectively improved contact area between LLTO NTs and PAN, which promotes the Lewis acid-base interaction for adsorbing anions and boosts Li^+ conductivity in LLTO NTs/PAN CSEs.^{25,31}

Apart from high ionic conductivity, another important performance parameter of solid electrolytes is their remarkable mechanical strength, which is essential to suppress the growth of lithium dendrites and to withstand external mechanical load.⁴¹ The stress–strain test (Figure 3e) shows that the tensile strength of the LLTO NTs/PAN CSE is 5.61 MPa, which is much higher than 2.93 MPa of the bare PAN solid electrolyte. Besides, the strain of the LLTO NTs/PAN CSE before breaking could reach up to 33%, whereas for the bare PAN solid electrolyte it was only 12.5%. The results indicate that the mechanical properties of as-prepared solid electrolytes can be significantly improved owing to the incorporation of mechanically robust LLTO NTs, which is key to realizing high-safety solid-state batteries.⁴² Furthermore, the thermal stability of the LLTO NTs/PAN CSE was studied by thermogravimetric analysis (TGA). Both LLTO NTs/PAN CSE and bare PAN solid electrolyte show similar thermodynamic stability in air before the temperature reaches around 350 °C (Figure S6). To further test their thermal stability in practical application, both kinds of solid electrolytes were heated at different temperatures in a glove box. Digital photographs (Figure S7) display shape changes of the LLTO NTs/PAN CSE and bare PAN solid electrolyte before and after 150 °C for 20 min, demonstrating that the LLTO NTs/PAN CSE can maintain the same shape, while the bare PAN solid electrolyte appears

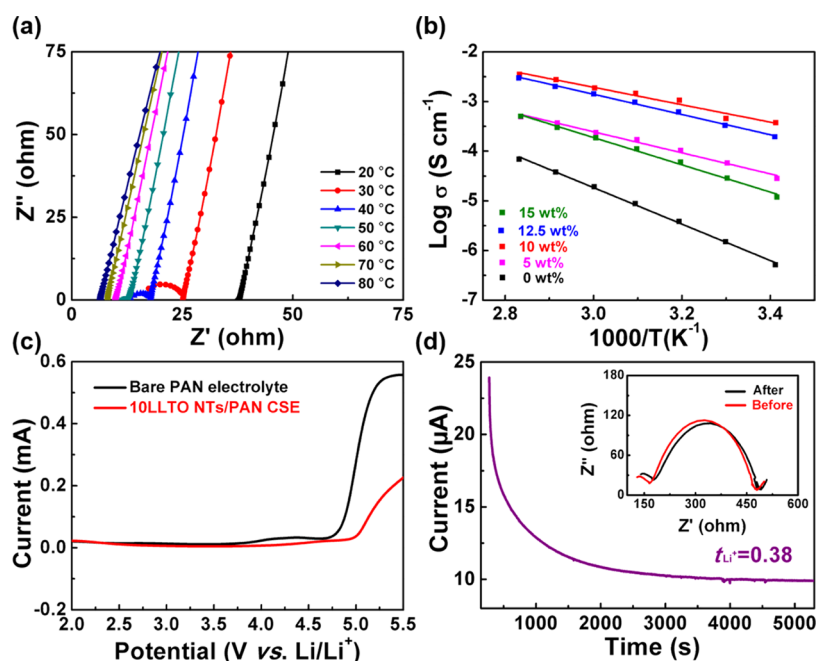


Figure 4. Electrochemical performance of the LLTO NTs/PAN CSEs. (a) EIS profiles of the 10LLTO NTs/PAN CSE at different temperatures. (b) Arrhenius plots of LLTO NTs/PAN CSEs with different concentrations of LLTO NTs. (c) Linear sweep voltammetry (LSV) curves of the 10LLTO NTs/PAN CSE and bare PAN solid electrolyte. (d) Current-time profile for the 10LLTO NTs/PAN CSE (the inset shows EIS variation before and after polarization).

to undergo an obvious shrinkage. Accordingly, the LLTO NTs/PAN CSE has excellent thermal stability and mechanical properties, which are beneficial for the safe performance of solid-state batteries.

The ionic conductivity was characterized by electrochemical impedance spectroscopy (EIS). Figure 4a shows the EIS curves of the 10LLTO NTs/PAN CSE at different temperatures. It can be calculated that its ionic conductivity reaches $3.6 \times 10^{-4} \text{ S cm}^{-1}$ at room temperature, which is three orders of magnitude higher than that of the bare PAN solid electrolyte ($6.8 \times 10^{-7} \text{ S cm}^{-1}$). Meanwhile, the ionic conductivity of the 10LLTO NTs/PAN CSE (at RT) is also higher than those of previously reported solid electrolytes with different structures of LLTO fillers (Table S1), which can be attributed to the open structure with 3D accessible Li^+ transport pathways. Moreover, as a typical A-site-deficient ion conductor, LLTO NTs with a larger specific surface area provide more vacancies, which facilitates the faster hop of lithium ions along their one-dimensional surface. Apart from this, lithium ion conduction in composite solid electrolytes is also controlled by polymer/filler interfacial interaction regions.^{33,35} Based on Lewis acid-base theory, a large number of ClO_4^- groups are restricted to the surface of LLTO nanotubes, so that the concentration of free Li^+ at the nanotube/polymer interface can be increased.^{16,43} Therefore, the large interface regions formed by LLTO NT's areas can enable fast ion conduction along the surface regions of nanotubes, improving the ionic conductivity of the as-obtained solid electrolyte.

Figure 4b shows the temperature-dependent (20–80 °C) Arrhenius plots for LLTO NTs/PAN CSEs with different contents of LLTO NTs, and an improvement of ionic conductivity could be achieved in all LLTO NTs/PAN CSEs compared with bare PAN solid electrolyte. After the fitting analysis for the obtained results, the corresponding activation energies of LLTO NTs/PAN CSEs with 0–15 wt % LLTO

NTs were 0.31, 0.2, 0.13, 0.16, and 0.23 eV, respectively. The decreased activation energy indicates that the introduction of LLTO NTs facilitates Li ion transport in the as-obtained solid electrolytes. The lowest activation energy of the 10LLTO NTs/PAN CSE indicates that 10 wt % LLTO NTs in the PAN-based electrolyte is the optimal amount for the transport of lithium ions. This result is consistent with the test in Figure S8, which shows that the conductivity of solid electrolytes increases with the addition of LLTO NTs, reaching the peak at 10 wt %, and begins to rapidly decline at 15 wt %. Apart from ionic conductivity, good electrochemical stability is also an important factor for the application of CSEs in solid-state batteries. To investigate this parameter, linear sweep voltammetry (LSV) testing results of the 10LLTO NTs/PAN CSE at the scan rate of 0.01 mV s^{-1} are shown in Figure 4c. Compared with the bare PAN solid electrolyte, the introduction of LLTO NTs improves the electrochemical stability of the 10LLTO NTs/PAN CSE up to 5 V, which holds great potential to match high-voltage cathodes for higher energy density. The improved electrochemical stability can be attributed to the high electrochemical stability of LLTO NTs. Moreover, impurities such as water may be removed from the polymer matrix by the LLTO ceramic nanotubes, which is beneficial to enhance the electrochemical window of LLTO NTs/PAN CSEs.^{44,45} According to Figure 4d, the Li^+ transference number (t_{Li^+}) of the 10LLTO NTs/PAN CSE is 0.38, which is higher than those of the bare PAN solid electrolyte ($t_{\text{Li}^+} = 0.15$ in Figure S9) and PAN-based composite solid electrolytes with LLTO nanowires ($t_{\text{Li}^+} = 0.26$ in Figure S9). The enhanced t_{Li^+} could be attributed to the LLTO NT's ceramic phase and the large nanotube/polymer interfacial interaction regions, which enable sufficient free lithium ions to reach electrodes.

Galvanostatic cycling was used to test the durability of the 10LLTO NTs/PAN CSE (Figure 5a) and the bare PAN solid

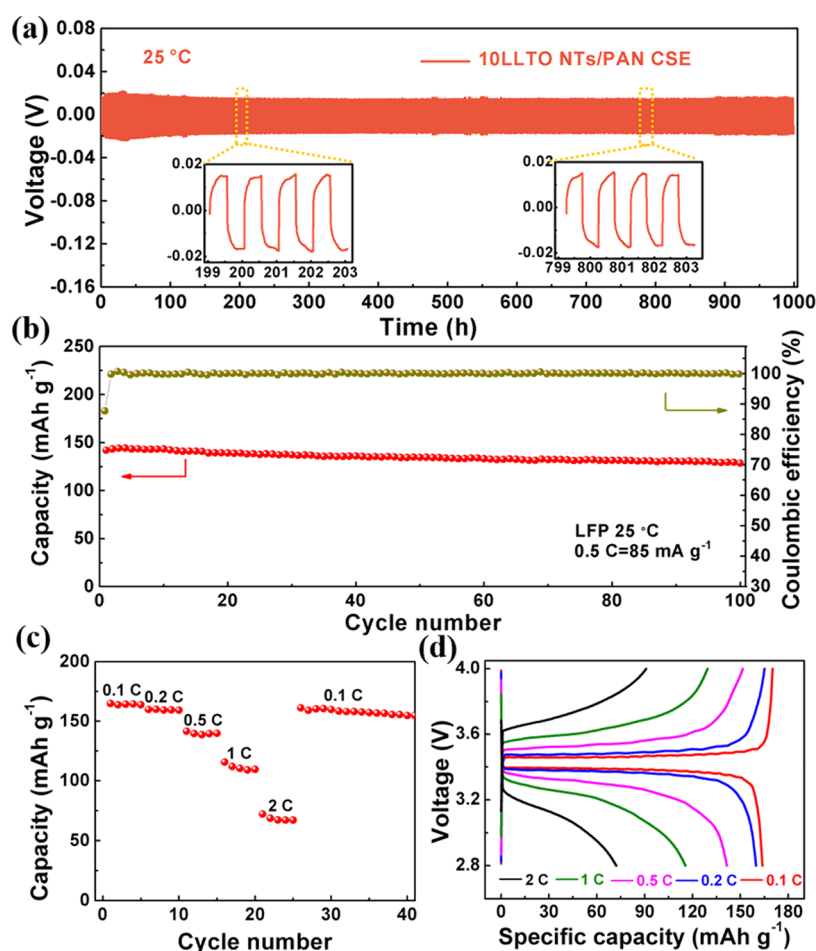


Figure 5. Electrochemical performance test of the 10LLTO NTs/PAN CSE in batteries. (a) Voltage profile of the continued lithium plating/stripping cycling with a current density of 0.05 mA cm^{-2} at RT (the inset shows the voltage profile around 200 h and 800 h). (b) Cycle stability with Coulombic efficiency under 0.5 C of the Li-LFP battery. (c) Rate capability (0.1–2 C) of the Li-LFP battery. (d) Corresponding charge-discharge voltage profiles.

electrolyte (Figure S10). The symmetric Li-Li battery with the 10LLTO NTs/PAN CSE shows a long-term stable operation over 1000 h with a small polarized voltage within 0.02 V, which is much lower than 0.5 V of the bare PAN solid electrolyte (within 200 h). Figure S11 shows the voltage profile of Li/10LLTO NTs/PAN CSE/Li under different current densities. The assembled Li-Li symmetric cell is stable and the overpotential value varies linearly with the current density. This fact demonstrates that the 10LLTO NTs/PAN CSE can effectively suppress the uneven Li deposition and the formation of Li dendrites so that few lithium dendrites existed on the lithium metal surface after cycling (Figure S12), which could be attributed to a synergistic effect between uniformly distributed LLTO NTs and enhanced mechanical properties of the 10LLTO NTs/PAN CSE.

The practical applicability of the 10LLTO NTs/PAN CSE was demonstrated by assembling full cells based on Li metal and LiFePO_4 (LFP) with the 10LLTO NTs/PAN CSE. To improve the contact between the solid electrolyte and the electrodes, a small amount of liquid electrolyte ($\sim 4 \mu\text{L cm}^{-2}$) was added to the electrolyte/electrode interfaces to reduce the interface resistance. Figure 5b presents the cycling performance of the Li-LFP battery between 2.8 and 4.0 V at 0.5 C, showing a stable discharge capacity of 142.5 mAh g^{-1} and maintaining 90% after 100 cycles. Apart from this, the discharge-specific

capacities are about 164.8, 159.8, 141.5, 115.5, and 72.2 mAh g^{-1} at 0.1, 0.2, 0.5, 1, and 2 C, respectively (Figure 5c,d). The initial value of capacity can be approached again as the rate returns to 0.1 C, which further proves the reversibility and stability of this solid-state battery. In addition, the 10LLTO NTs/PAN CSE also shows great stability when applied to a Li-NCM811 battery between 3.0 and 4.3 V at 0.5 C (Figure S13).

4. CONCLUSIONS

In summary, unique open-structured LLTO NTs were successfully prepared by a gradient electrospinning strategy as fillers in solid electrolytes. Different from nanoparticles and nanowires, our nanotubes are composed of connected small NPs and form many pores and channels among them. The as-obtained solid electrolytes achieve an ionic conductivity of $3.6 \times 10^{-4} \text{ S cm}^{-1}$ and a Li^+ transference number of 0.38, owing to more Li^+ transport pathways together with the large interfacial ion conduction area and enhanced nanotube/polymer interaction. In addition to improved transportation of lithium ions, the LLTO NTs/PAN CSE has good thermal stability and high mechanical strength (tensile strength of 5.61 MPa), as well as a wide electrochemical window of 5 V. The Li-Li symmetric cells with the LLTO NTs/PAN CSE can achieve long-term cycle stability without a short circuit. Solid batteries assembled with Li/10LLTO NTs/PAN CSE/LiFePO₄ show a

good cycling performance and rate capacity at RT. All of the results indicate that the rational design of open-structured nanotubes establishes a potential way for advanced nano-structured fillers, which can be applied in high-performance solid electrolytes for solid-state lithium metal batteries.

■ ASSOCIATED CONTENT

SI Supporting Information

The Supporting Information is available free of charge at <https://pubs.acs.org/doi/10.1021/acsami.0c22635>.

Details for structural and electrochemical characterizations; SEM images of LLTO nanotubes at different calcination temperatures; SEM images of the Li metal surface before and after cycling; TGA curves of different molecular-weight PVP and LLTO NTs/PAN CSEs from 35 to 800 °C; XRD patterns of LLTO NTs; BET result of LLTO with different structures; Li ion transference number and ionic conductivity of as-obtained solid electrolytes; and charge/discharge profiles of full batteries based on a high-voltage cathode (PDF)

■ AUTHOR INFORMATION

Corresponding Author

Lin Xu – State Key Laboratory of Advanced Technology for Materials Synthesis and Processing, School of Materials Science and Engineering, Wuhan University of Technology, Wuhan 430070, Hubei, P. R. China; Foshan Xianhu Laboratory of the Advanced Energy Science and Technology Guangdong Laboratory, Xianhu Hydrogen Valley, Foshan 528200, Guangdong, P. R. China; orcid.org/0000-0003-2347-288X; Email: linxu@whut.edu.cn

Authors

Song Hu – State Key Laboratory of Advanced Technology for Materials Synthesis and Processing, School of Materials Science and Engineering, Wuhan University of Technology, Wuhan 430070, Hubei, P. R. China

Lulu Du – State Key Laboratory of Advanced Technology for Materials Synthesis and Processing, School of Materials Science and Engineering, Wuhan University of Technology, Wuhan 430070, Hubei, P. R. China

Gang Zhang – State Key Laboratory of Advanced Technology for Materials Synthesis and Processing, School of Materials Science and Engineering, Wuhan University of Technology, Wuhan 430070, Hubei, P. R. China

Wenyuan Zou – State Key Laboratory of Advanced Technology for Materials Synthesis and Processing, School of Materials Science and Engineering, Wuhan University of Technology, Wuhan 430070, Hubei, P. R. China

Zhe Zhu – State Key Laboratory of Advanced Technology for Materials Synthesis and Processing, School of Materials Science and Engineering, Wuhan University of Technology, Wuhan 430070, Hubei, P. R. China

Liqiang Mai – State Key Laboratory of Advanced Technology for Materials Synthesis and Processing, School of Materials Science and Engineering, Wuhan University of Technology, Wuhan 430070, Hubei, P. R. China; Foshan Xianhu Laboratory of the Advanced Energy Science and Technology Guangdong Laboratory, Xianhu Hydrogen Valley, Foshan 528200, Guangdong, P. R. China; orcid.org/0000-0003-4259-7725

Complete contact information is available at:

<https://pubs.acs.org/10.1021/acsami.0c22635>

Author Contributions

S.H. and L.D. contributed equally to this work.

Notes

The authors declare no competing financial interest.

■ ACKNOWLEDGMENTS

This work was supported by the National Natural Science Foundation of China (51802239), the National Key Research and Development Program of China (2020YFA0715000), the Foshan Xianhu Laboratory of the Advanced Energy Science and Technology Guangdong Laboratory (XHT2020-005, XHT2020-003), the Natural Science Foundation of Hubei Province (2019CFA001), the National Key Research and Development Program of China (2019YFA0704902), and the Fundamental Research Funds for the Central Universities (2020III011GX, 2020IVB057, 2019IVB054, and 2019III062JL).

■ REFERENCES

- (1) Manthiram, A.; Yu, X.; Wang, S. Lithium Battery Chemistries Enabled by Solid-State Electrolytes. *Nat. Rev. Mater.* **2017**, *2*, No. 16103.
- (2) Zhu, Z.; Kan, R.; Hu, S.; He, L.; Hong, X.; Tang, H.; Luo, W. Recent Advances in High-Performance Microbatteries: Construction, Application, and Perspective. *Small* **2020**, *16*, No. 2003251.
- (3) Liu, J.; Bao, Z.; Cui, Y.; Dufek, E. J.; Goodenough, J. B.; Khalifah, P.; Li, Q.; Liaw, B. Y.; Liu, P.; Manthiram, A.; Meng, Y. S.; Subramanian, V. R.; Toney, M. F.; Viswanathan, V. V.; Whittingham, M. S.; Xiao, J.; Xu, W.; Yang, J.; Yang, X.-Q.; Zhang, J.-G. Pathways for Practical High-Energy Long-Cycling Lithium Metal Batteries. *Nat. Energy* **2019**, *4*, 180–186.
- (4) Yang, C.; Fu, K.; Zhang, Y.; Hitz, E.; Hu, L. Protected Lithium-Metal Anodes in Batteries: From Liquid to Solid. *Adv. Mater.* **2017**, *29*, No. 1701169.
- (5) Fan, L.; Wei, S.; Li, S.; Li, Q.; Lu, Y. Recent Progress of the Solid-State Electrolytes for High-Energy Metal-Based Batteries. *Adv. Energy Mater.* **2018**, *8*, No. 1702657.
- (6) Goodenough, J. B.; Singh, P. Review—Solid Electrolytes in Rechargeable Electrochemical Cells. *J. Electrochem. Soc.* **2015**, *162*, 2387–2392.
- (7) Thangadurai, V.; Narayanan, S.; Pinzaru, D. Garnet-type Solid-State Fast Li Ion Conductors for Li Batteries: Critical Review. *Chem. Soc. Rev.* **2014**, *43*, 4714–4727.
- (8) Xia, S.; Wu, X.; Zhang, Z.; Cui, Y.; Liu, W. Practical Challenges and Future Perspectives of All-Solid-State Lithium-Metal Batteries. *Chem* **2019**, *5*, 753–785.
- (9) Chen, R.; Qu, W.; Guo, X.; Li, L.; Wu, F. The Pursuit of Solid-State Electrolytes for Lithium Batteries: from Comprehensive Insight to Emerging Horizons. *Mater. Horiz.* **2016**, *3*, 487–516.
- (10) Dong, D.; Zhou, B.; Sun, Y.; Zhang, H.; Zhong, G.; Dong, Q.; Fu, F.; Qian, H.; Lin, Z.; Lu, D.; Shen, Y.; Wu, J.; Chen, L.; Chen, H. Polymer Electrolyte Glue: A Universal Interfacial Modification Strategy for All-Solid-State Li Batteries. *Nano Lett.* **2019**, *19*, 2343–2349.
- (11) Yue, L.; Ma, J.; Zhang, J.; Zhao, J.; Dong, S.; Liu, Z.; Cui, G.; Chen, L. All Solid-State Polymer Electrolytes for High-Performance Lithium Ion Batteries. *Energy Storage Mater.* **2016**, *5*, 139–164.
- (12) Zhao, N.; Khokhar, W.; Bi, Z.; Shi, C.; Guo, X.; Fan, L.-Z.; Nan, C.-W. Solid Garnet Batteries. *Joule* **2019**, *3*, 1190–1199.
- (13) Duan, H.; Fan, M.; Chen, W. P.; Li, J. Y.; Wang, P. F.; Wang, W. P.; Shi, J. L.; Yin, Y. X.; Wan, L. J.; Guo, Y. G. Extended Electrochemical Window of Solid Electrolytes via Heterogeneous Multilayered Structure for High-Voltage Lithium Metal Batteries. *Adv. Mater.* **2019**, *31*, No. 1807789.

- (14) Duan, H.; Chen, W. P.; Fan, M.; Wang, W. P.; Yu, L.; Tan, S. J.; Chen, X.; Zhang, Q.; Xin, S.; Wan, L. J.; Guo, Y. G. Building an Air Stable and Lithium Deposition Regulable Garnet Interface from Moderate-Temperature Conversion Chemistry. *Angew. Chem., Int. Ed.* **2020**, *59*, 12069–12075.
- (15) Chi, S.-S.; Liu, Y.; Zhao, N.; Guo, X.; Nan, C.-W.; Fan, L.-Z. Solid Polymer Electrolyte Soft Interface Layer with 3D Lithium Anode for All-Solid-State Lithium Batteries. *Energy Storage Mater.* **2019**, *17*, 309–316.
- (16) Huang, Y.; Chen, B.; Duan, J.; Yang, F.; Wang, T.; Wang, Z.; Yang, W.; Hu, C.; Luo, W.; Huang, Y. Graphitic Carbon Nitride ($g\text{-C}_3\text{N}_4$): An Interface Enabler for Solid-State Lithium Metal Batteries. *Angew. Chem., Int. Ed.* **2020**, *59*, 3699–3704.
- (17) Liu, W.; Lee, S. W.; Lin, D.; Shi, F.; Wang, S.; Sendek, A. D.; Cui, Y. Enhancing Ionic Conductivity in Composite Polymer Electrolytes with Well-Aligned Ceramic Nanowires. *Nat. Energy* **2017**, *2*, No. 17035.
- (18) Wang, X.; Zhai, H.; Qie, B.; Cheng, Q.; Li, A.; Borovilas, J.; Xu, B.; Shi, C.; Jin, T.; Liao, X.; Li, Y.; He, X.; Du, S.; Fu, Y.; Dontigny, M.; Zaghbi, K.; Yang, Y. Rechargeable Solid-State Lithium Metal Batteries with Vertically Aligned Ceramic Nanoparticle/Polymer Composite Electrolyte. *Nano Energy* **2019**, *60*, 205–212.
- (19) Bae, J.; Li, Y.; Zhang, J.; Zhou, X.; Zhao, F.; Shi, Y.; Goodenough, J. B.; Yu, G. A 3D Nanostructured Hydrogel-Framework-Derived High-Performance Composite Polymer Lithium-ion Electrolyte. *Angew. Chem., Int. Ed.* **2018**, *57*, 2096–2100.
- (20) Xie, H.; Yang, C.; Fu, K. K.; Yao, Y.; Jiang, F.; Hitz, E.; Liu, B.; Wang, S.; Hu, L. Flexible, Scalable, and Highly Conductive Garnet-Polymer Solid Electrolyte Templated by Bacterial Cellulose. *Adv. Energy Mater.* **2018**, *8*, No. 1703474.
- (21) Fu, K. K.; Gong, Y.; Dai, J.; Gong, A.; Han, X.; Yao, Y.; Wang, C.; Wang, Y.; Chen, Y.; Yan, C.; Li, Y.; Wachsman, E. D.; Hu, L. Flexible, Solid-State, Ion-Conducting Membrane with 3D Garnet Nanofiber Networks for Lithium Batteries. *Proc. Natl. Acad. Sci. U.S.A.* **2016**, *113*, 7094–7099.
- (22) Xia, Y.; Xu, N.; Du, L.; Cheng, Y.; Lei, S.; Li, S.; Liao, X.; Shi, W.; Xu, L.; Mai, L. Rational Design of Ion Transport Paths at the Interface of Metal-Organic Framework Modified Solid Electrolyte. *ACS Appl. Mater. Interfaces* **2020**, *12*, 22930–22938.
- (23) Croce, F.; Appetecchi, G. B.; Persi, L.; Scrosati, B. Nanocomposite Polymer Electrolytes for Lithium Batteries. *Nature* **1998**, *394*, 456–458.
- (24) Hema, M.; Tamilselvi, P. Lithium Ion Conducting PVA: PVdF Polymer Electrolytes Doped with Nano SiO_2 and TiO_2 Filler. *J. Phys. Chem. Solids* **2016**, *96*–97, 42–48.
- (25) Lin, D.; Yuen, P. Y.; Liu, Y.; Liu, W.; Liu, N.; Dauskardt, R. H.; Cui, Y. A Silica-Aerogel-Reinforced Composite Polymer Electrolyte with High Ionic Conductivity and High Modulus. *Adv. Mater.* **2018**, *30*, No. 1802661.
- (26) Zhai, H.; Xu, P.; Ning, M.; Cheng, Q.; Mandal, J.; Yang, Y. A Flexible Solid Composite Electrolyte with Vertically Aligned and Connected Ion-Conducting Nanoparticles for Lithium Batteries. *Nano Lett.* **2017**, *17*, 3182–3187.
- (27) Dai, J.; Fu, K.; Gong, Y.; Song, J.; Chen, C.; Yao, Y.; Pastel, G.; Zhang, L.; Wachsman, E.; Hu, L. Flexible Solid-State Electrolyte with Aligned Nanostructures Derived from Wood. *ACS Mater. Lett.* **2019**, *1*, 354–361.
- (28) Bae, J.; Li, Y.; Zhao, F.; Zhou, X.; Ding, Y.; Yu, G. Designing 3D Nanostructured Garnet Frameworks for Enhancing Ionic Conductivity and Flexibility in Composite Polymer Electrolytes for Lithium Batteries. *Energy Storage Mater.* **2018**, *15*, 46–52.
- (29) Liu, W.; Liu, N.; Sun, J.; Hsu, P. C.; Li, Y.; Lee, H. W.; Cui, Y. Ionic Conductivity Enhancement of Polymer Electrolytes with Ceramic Nanowire Fillers. *Nano Lett.* **2015**, *15*, 2740–2745.
- (30) Yu, J.; Wang, C.; Li, S.; Liu, N.; Zhu, J.; Lu, Z. Li^+ -Containing, Continuous Silica Nanofibers for High Li^+ Conductivity in Composite Polymer Electrolyte. *Small* **2019**, *15*, No. 1902729.
- (31) Ni, Q.; Bai, Y.; Li, Y.; Ling, L.; Li, L.; Chen, G.; Wang, Z.; Ren, H.; Wu, F.; Wu, C. 3D Electronic Channels Wrapped Large-Sized $\text{Na}_3\text{V}_2(\text{PO}_4)_3$ as Flexible Electrode for Sodium-Ion Batteries. *Small* **2018**, *14*, No. 1702864.
- (32) Zhang, X.; Xie, J.; Shi, F.; Lin, D.; Liu, Y.; Liu, W.; Pei, A.; Gong, Y.; Wang, H.; Liu, K.; Xiang, Y.; Cui, Y. Vertically Aligned and Continuous Nanoscale Ceramic-Polymer Interfaces in Composite Solid Polymer Electrolytes for Enhanced Ionic Conductivity. *Nano Lett.* **2018**, *18*, 3829–3838.
- (33) Yang, T.; Zheng, J.; Cheng, Q.; Hu, Y. Y.; Chan, C. K. Composite Polymer Electrolytes with $\text{Li}_7\text{La}_3\text{Zr}_2\text{O}_{12}$ Garnet-Type Nanowires as Ceramic Fillers: Mechanism of Conductivity Enhancement and Role of Doping and Morphology. *ACS Appl. Mater. Interfaces* **2017**, *9*, 21773–21780.
- (34) Zekoll, S.; Marriner-Edwards, C.; Hekselman, A. K. O.; Kasemchainan, J.; Kuss, C.; Armstrong, D. E. J.; Cai, D.; Wallace, R. J.; Richter, F. H.; Thijssen, J. H. J.; Bruce, P. G. Hybrid Electrolytes with 3D Bicontinuous Ordered Ceramic and Polymer Microchannels for All-Solid-State Batteries. *Energy Environ. Sci.* **2018**, *11*, 185–201.
- (35) Hu, C.; Shen, Y.; Shen, M.; Liu, X.; Chen, H.; Liu, C.; Kang, T.; Jin, F.; Li, L.; Li, J.; Li, Y.; Zhao, N.; Guo, X.; Lu, W.; Hu, B.; Chen, L. Superionic Conductors via Bulk Interfacial Conduction. *J. Am. Chem. Soc.* **2020**, *142*, 18035–18041.
- (36) Niu, C.; Meng, J.; Wang, X.; Han, C.; Yan, M.; Zhao, K.; Xu, X.; Ren, W.; Zhao, Y.; Xu, L.; Zhang, Q.; Zhao, D.; Mai, L. General Synthesis of Complex Nanotubes by Gradient Electrospinning and Controlled Pyrolysis. *Nat. Commun.* **2015**, *6*, No. 7402.
- (37) Shin, Y.; Hohman, M.; Brenner, M.; Rutledge, G. Experimental Characterization of Electrospinning: the Electrically Forced Jet and Instabilities. *Polymer* **2011**, *42*, 9955–9967.
- (38) Fridrikh, S. V.; Yu, J. H.; Brenner, M. P.; Rutledge, G. C. Controlling the Fiber Diameter During Electrospinning. *Phys. Rev. Lett.* **2003**, *90*, No. 144502.
- (39) Stramare, S.; Thangadurai, V.; Weppner, W. Lithium Lanthanum Titanates: A Review. *Chem. Mater.* **2003**, *34*, 3974–3990.
- (40) Xin, B.; Hao, J. Reversibly Switchable Wettability. *Chem. Soc. Rev.* **2010**, *39*, 769–782.
- (41) Khurana, R.; Schaefer, J. L.; Archer, L. A.; Coates, G. W. Suppression of Lithium Dendrite Growth Using Cross-Linked Polyethylene/Poly(ethylene oxide) Electrolytes: a New Approach for Practical Lithium-Metal Polymer Batteries. *J. Am. Chem. Soc.* **2014**, *136*, 7395–7402.
- (42) Zhang, J.; Zhang, X.; Wen, H.; Dong, T.; Chai, J.; Li, Y.; Chen, B.; Zhao, J.; Dong, S.; Ma, J.; Yue, L.; Liu, Z.; Guo, X.; Cui, G.; Chen, L. High-Voltage and Free-Standing Poly(propylene carbonate)/ $\text{Li}_{6.75}\text{La}_3\text{Zr}_{1.75}\text{Ta}_{0.25}\text{O}_{12}$ Composite Solid Electrolyte for Wide Temperature Range and Flexible Solid Lithium Ion Battery. *J. Mater. Chem. A* **2017**, *5*, 4940–4948.
- (43) Wang, Z.; Huang, X.; Chen, L. Understanding of Effects of Nano- Al_2O_3 Particles on Ionic Conductivity of Composite Polymer Electrolytes. *Electrochem. Solid-State Lett.* **2003**, *6*, 1746.
- (44) Zhang, J.; Zhao, N.; Zhang, M.; Li, Y.; Chu, P. K.; Guo, X.; Di, Z.; Wang, X.; Li, H. Flexible and Ion-Conducting Membrane Electrolytes for Solid-State Lithium Batteries: Dispersion of Garnet Nanoparticles in Insulating Polyethylene Oxide. *Nano Energy* **2016**, *28*, 447–454.
- (45) Wang, X.; Zhang, Y.; Zhang, X.; Liu, T.; Lin, Y. H.; Li, L.; Shen, Y.; Nan, C. W. Lithium-Salt-Rich PEO/ $\text{Li}_{0.3}\text{La}_{0.557}\text{TiO}_3$ Interpenetrating Composite Electrolyte with Three-Dimensional Ceramic Nano-Backbone for All-Solid-State Lithium-Ion Batteries. *ACS Appl. Mater. Interfaces* **2018**, *10*, 24791–24798.